Talanta 207 (2020) 120311

Contents lists available at ScienceDirect

Talanta

journal homepage: www.elsevier.com/locate/talanta

A novel bimacrocyclic polyamine-based fluorescent probe for sensitive detection of Hg^{2+} and glutathione in human serum

Xiaobo Wang[a,b], Xiaoyan Ma[a], Jinghan Wen[a], Zhirong Geng[a,**], Zhilin Wang[a,*]

[a] State Key Laboratory of Coordination Chemistry, School of Chemistry and Chemical Engineering, Collaborative Innovation Center of Advanced Microstructures, Nanjing University, Nanjing, 210023, PR China

[b] Pharmacy School, Hubei University of Science and Technology, Xianning, 437100, PR China

ARTICLE INFO

Keywords:
Mercury
Fluorescent probe
GSH
Golgi apparatus
Human serum

ABSTRACT

Detection of glutathione in human serum is of great importance for clinical diagnosis of various diseases, such as AIDS, diabetes mellitus, Alzheimer disease and cancer. In this work, a new water-soluble bismacrocyclic polyamine-derived compound, namely L, which contains two molecules of 4-nitro-1,2,3-benzoxa-diazole as the fluorophores, was designed and prepared. The experiments of selectivity of L toward metal ions showed it could rapidly and sensitively detect Hg^{2+} with a detection limit of 27 nM. Furthermore, the cell imaging and co-staining experiments in HeLa cells demonstrated that the L-Hg^{2+} probe had selectivity for the Golgi apparatus to a certain degree. Moreover, it had excellent selectivity for biothiols, especially for glutathione. Finally, the probe was successfully applied to sensitively detect glutathione (GSH) in human serum and fetal bovine serum.

1. Introduction

Mercury is a highly poisonous neurological toxin. It is also considered as a hazardous heavy metal pollutant due to its widely use in many fields. Inorganic mercury (Hg^{2+}) can be converted to a more toxic organic form i.e. methylmercury (MeHg) by sulfate-reducing bacteria (SRB) [1–3]. The MeHg can subsequently be accumulated in the human body, especially in the central nervous system, through the food chain [4–7]. Paddy rice and fish consumption is the main source of mercury exposure in populations living in Chinese mainland. In a vast area of some regions, such as Guizhou province, paddy fields and water sources have been severely contaminated by mercury [8–11].

Mercury is also a highly thiophilic metal that has strong affinity for thiol-containing biomolecules (biothiols), such as GSH, cysteine (Cys), homocysteine (Hcy), and albumin. It is widely known that the formation constant for Hg(II)-thiol bond has been estimated to be as much as 10 orders of magnitude greater than the formation constant for the bonding of Hg(II) to other nucleophiles present under the same condition [12,13]. This is the reason that them play vital roles in maintaining the appropriate redox status of biological systems. Among these biothiols, GSH is the most abundant endogenous nonprotein thiol and its cellular concentrations can range from 1 to 15 mM depending on the cell types [14,15]. Of all the thiol containing components of blood, the GSH conent makes up approximately 90% of its entire composition with previous literature stating that, owing to this extremely high concentration of GSH, all other potential thiol molecules can be ignored [16,17]. The aberrant concentration of GSH in serum has been reported to link with many medical conditions including edema, skin lesions and slow growth of children [18,19]. GSH is also well-known as a scavenger protecting the cells against reactive oxygen species (ROS), drugs, and heavy metal ions (including Hg^{2+}) [20,21]. It is involved in the regulation of the redox homeostasis through the equilibrium between its reduced form (GSH) and GSSG.

Based on above, it is of great significance to develop a simple and sensitive detection of aqueous Hg^{2+}. Fluorescent probes are powerful tools in the study of function, metabolism or toxicity of metals and biological molecules at the molecular level, in addition to environmental monitoring. Many small molecule-based fluorescent probes have been developed for detecting Hg^{2+} in aqueous solution [22–28], some of which have succeeded in cells and vertebrate models, such as zebrafish [26–28]. A plentiful of probes for Hg^{2+} detection are constituted by a fluorophore containing nitrogen receptor units [27,29–33]. This implies that nitrogen containing macrocyclic receptors are suitable for constructing Hg^{2+} probes. Meanwhile, our group has been devoting ourselves to the design and use of N-containing macrocycles for fluorescent probes in recent years [34,35].

Consequently, it is feasible to design fluorescent probes for Hg^{2+} recognization based on N-containing macrocycles and followed by

* Corresponding author.
** Corresponding author. Tel.: +86-25-89689007; fax: +86-25-89687761.
E-mail addresses: gengzr@nju.edu.cn (Z. Geng), wangzl@nju.edu.cn (Z. Wang).

https://doi.org/10.1016/j.talanta.2019.120311
Received 6 June 2019; Received in revised form 24 August 2019; Accepted 2 September 2019
Available online 05 September 2019
0039-9140/

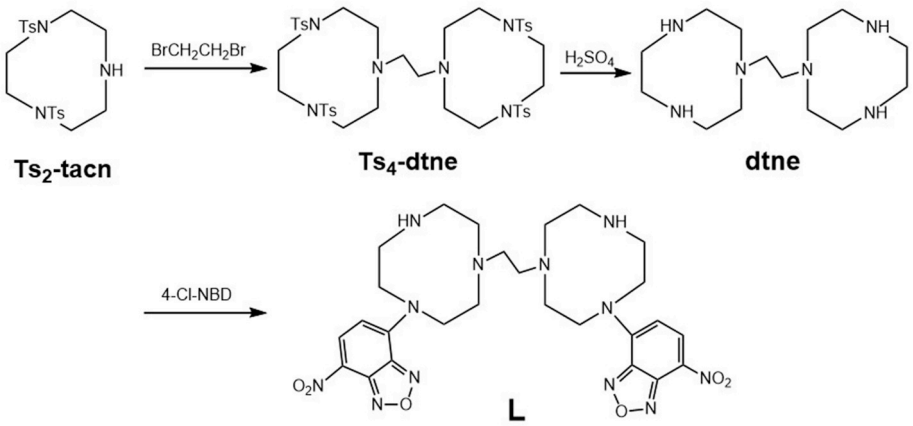

Scheme 1. Synthetic route of probe L.

biothiols detection on the basis of strong bond affinity between Hg and sulfydryl of GSH [36]. In this work, the fluorescent probe L, bearing two 1,4,7-triazacyclononane as receptors was synthesized and used to detect Hg^{2+}. This probe responds to Hg^{2+} rapidly and sensitively with the limit of detection (LOD) of 27 nM. Cell imaging experiments demonstrated L is a subcellular localization probe on Golgi apparatus. Furthermore, the L-Hg^{2+} complex was successfully applied to detect GSH in human serum employing standard addition method.

2. Experimental

2.1. Reagents and instrumentation

All starting materials were of reagent quality and were obtained from commercial sources. They were used without further purification. 4-chloro-7-nitro-1,2,3-benzoxa-diazole (4-Cl-NBD), N-ethylmaleimide and N-acetyl-L-cysteine were purchased from Heowns Co., Ltd. MTT was obtained from Sigma-Aldrich Co., Ltd. Hoechst 33358, Mitotracker Red, BODIPY TR ceramide, LysoTracker Red DND-99 were purchased from Invitrogen Co., Ltd. Human serum and fetal bovine serum (FBS) were obtained from Nanjing First Hospital and Gibco company, respectively.

Electrospray ionization (ESI) mass spectra were obtained using a LCQ Fleet ThermoFisher mass spectrometer. All emission spectra were recorded on a PerkinElmer LS 55 fluorescence spectrometer. ^{1}H NMR spectra in $CDCl_3$ were measured using a Bruker DRX-500 spectrometer at 25 ± 1 °C. Sample pH was monitored using a PHS-3 system. Temperature in fluorescence titration was controlled using a LAUDA E100 circulating water pump. Analysis of MTT assay was conducted using a microplate reader (Thermo Scientific Varioskan Flash, USA). Fluorescence cell imaging was carried out using a CarlZeiss LSM 710 confocal microscope system (Germany).

2.2. Synthesis of compound L

The synthesis route of L is shown in Scheme 1. Ethyl-bridged bimacrocyclic polyamine compound **Ts_4-dtne** was synthetized by reacting between **Ts_2-tacn** and 1,2-dibromoethane. Then removing the protecting group Tosyl of **Ts_4-dtne** in concentrated H_2SO_4 gave the free bimacrocyclic polyamine **dtne** in 81% yield. After **dtne** reacted with 4-Cl-NBD in $CHCl_3$, the target compound L, with NBD-armed bimacrocyclic polyamine was obtained.

2.2.1. Synthesis of N,N′-bis(p-tolylsulfonyl)-1,4,7-triazacyclononane (*Ts_4-dtne*)

1,4-Bis(*p*-tolylsulfonyl)-1,4,7-triazacyclononane (**Ts_2-tacn**) was prepared according to the previous method [37–39]. **Ts_2-tacn** (4.8 g, 11 mmol) in 120 mL acetonitrile was mixed with Na_2CO_3 (4.81 g, 45 mmol) in 60 mL water and then stirred at 100 °C for 5 min. After 1,2-dibromoethane (0.5 mL, 5.5 mmol) was added, the mixture was refluxed for 24 h. And after cooling down to room temperature, it was poured into 300 mL of ice-cold water and vigorously stirred. The resultant mixture was filtered to obtain white solid precipitate, which was then washed three times with ice water (50 mL each) and dried under vacuum to afford the product **Ts_4-dtne** 4.4 g (89%). ESI-MS (CH_3CN): calculated *m/z* for $C_{42}H_{57}N_6O_8S_4$ [**Ts_4-dtne** + **H**]$^+$ was 901.30; measured value was 901.42 (Fig. S1, Supporting Information).

2.2.2. Synthesis of 1,2-bis(1,4,7-triaza-1-cyclononyl)ethane (*dtne*)

Ts_4-dtne (4.5 g) was dissolved in 20 mL of concentrated H_2SO_4, and while stirring, the mixture was heated at 100 °C for 60 h, which resulted in a yellow solution. After cooling down to room temperature, the mixture was added dropwise with pre-prepared cooled 20% NaOH (the resulting solution has a pH ≥ 13), and after that was filtered to remove $Na_2SO_4{\cdot}10H_2O$. The filtrate was extracted three times with $CHCl_3$ (50 mL each). The chloroform layers were combined and dried over anhydrous sodium sulfate overnight. After filtration, chloroform was removed under reduced pressure and to give the free polyamine **dtne**,

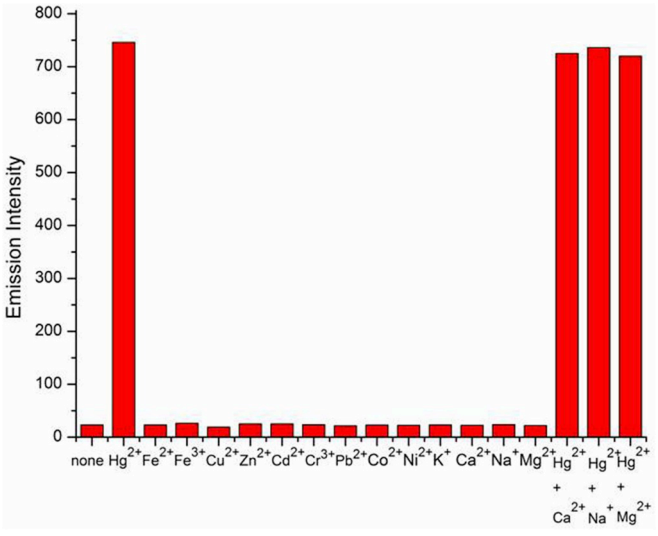

Fig. 1. Fluorescence emission intensity of L in the presences of different metal ions. The amount of Ca^{2+}, Na^+ and Mg^{2+} was 10 equivalence, and that of other ions was 1 mol equivalence. The measurement was carried out in 10 mM HEPES buffer, pH 7.4 containing 5% CH_3CN. [L] = 20 μM λ_{ex} = 470 nm λ_{em} = 530 nm.

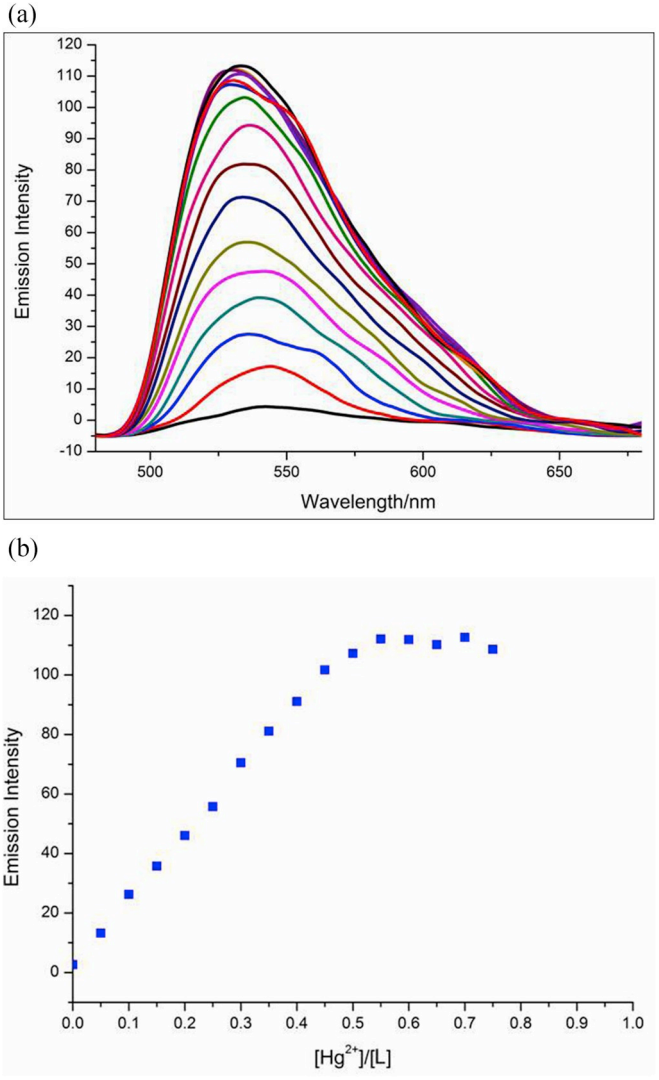

Fig. 2. (a) Fluorescence emission spectra of 20 μM L in 10 mM HEPES buffer, pH 7.4 containing 5% CH_3CN titrated with $Hg(ClO_4)_2$ solution (bottom to top: 0–15 μM). λ_{ex} = 470 nm. (b) Fluorescence titration profile extracted from (a).

pale yellow oil solidified as white crystalline solid on standing, was obtained (1.15 g, 81% yield). ESI-MS (CH_3CN): calculated *m/z* for $C_{14}H_{33}N_6$ [**dtne** + **H**]$^+$ was 285.45; the measured value was 285.58 (Fig. S1, Supporting Information).

2.2.3. Synthesis of 4,4′-bis(4-nitro-1,2,3-benzoxa-diazole)-1,2-bis(1,4,7-triaza-1- cyclononyl)ethane (L)

4-Chloro-7-nitro-1,2,3-benzoxa-diazole (852 mg, 3 mmol) in 50 mL of $CHCl_3$ was added dropwise to 100 mL of a solution containing **dtne** (618 mg, 3 mmol) and Et_3N (102 mg, 1 mmol) in $CHCl_3$. The resulting mixture was then heated at 60 °C and stirred for 2 h under N_2 ambient. After being cooled down to room temperature, the obtained mixture was washed three times with 1 M NaOH solution (20 mL each), followed by three times with redistilled water (3 × 20 mL). The organic layer was dried over anhydrous sodium sulfate overnight and evaporated to give the solid crude product. The residue was purified by column chromatography and eluted with a gradient of chloroform/methanol/$NH_3{\cdot}H_2O$ (v/v/v, 10:1:0.1), yielding a deep red solid, product L (115 mg, 38%). ESI-MS (CH_3CN): calculated *m/z* for $C_{26}H_{35}N_{12}O_6$ [L + H]$^+$ was 611.27; the measured value was 611.67 (Fig. S1, Supporting Information); ^{1}H NMR (500 MHz, $CDCl_3$) δ 8.48 (d, *J* = 8.9 Hz, 1H), 8.58 (s, 1 H), 8.09 (d, *J* = 8.3, 2 H), 7.63 (m, 2 H), 7.54 (d, *J* = 7.9, 2 H), 7.52 (m, 1 H), 6.17 (d, *J* = 9.0 Hz, 1H), 4.16 (d, *J* = 56.7 Hz, 4H), 3.26 (s, 2H), 3.11 (s, 2H), 2.70 (s, 2H), 2.58 (s, 2H), 2.51 (s, 2H), 1.28 (s, 4H) (Fig. S2, Supporting Information).

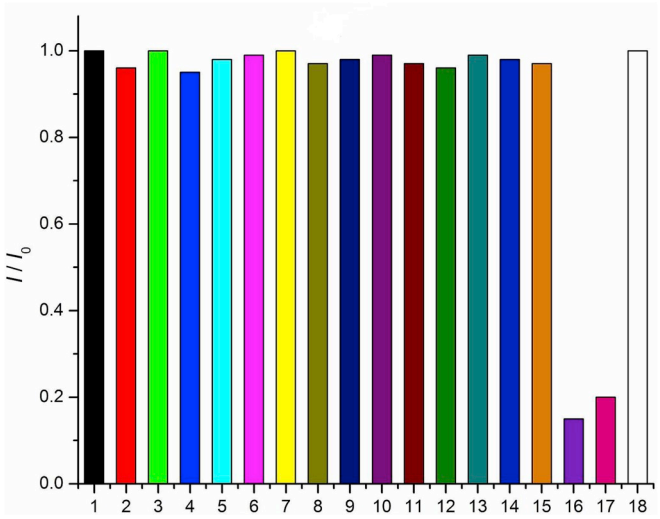

Fig. 3. Fluorescence changes of L-Hg^{2+} (20 μM) in the presence of different ions, amino acids and other compounds. One mole equivalence of sodium salts, except for Br^- and I^-, which were used as potassium salts. The measurement was conducted in 10 mM HEPES buffer, pH 7.4 containing 5% CH_3CN. 1 represent control group, 2 to 18 represent F^-, Cl^-, Br^-, CH_3COO^-, CO_3^{2-}, NO_3^-, PO_4^{3-}, SO_4^{2-}, PPi, glycine, histidine, aspartic acid, tyrosine, threonine, GSH, Cys, and GSSG, respectively.

2.3. Solution preparation

Stock solutions (20 mM) of metal ions, including Na^+, K^+, Ca^{2+}, Mg^{2+}, Zn^{2+}, Cu^{2+}, Fe^{3+}, Fe^{2+}, Co^{2+}, Ni^{2+}, Cd^{2+}, Pb^{2+}, Cr^{3+}, and Hg^{2+}, were prepared in deionized water. Stock solution of L was prepared by dissolving L in 10 mM HEPES buffer, pH 7.4 containing 5% CH_3CN. Stock solutions (10 mM) of anions (NaF, NaCl, KBr, CH_3COONa, Na_2CO_3, KNO_3, Na_2SO_4, Na_3PO_4, $Na_4P_2O_7$, glycine, histidine, aspartic acid, tyrosine, threonine, GSH, cysteine, and GSSG) were also prepared in deionized water.

2.4. Cell culture and MTT assay

HeLa cells were cultured and maintained in Dulbecco's modified Eagle's medium (DMEM) containing 10% fetal bovine serum (Gibco) and antibiotics (100 units/mL penicillin and 100 μg/mL streptomycin) at 37 °C in an incubator humidified with 5% CO2. Before MTT assay, HeLa cells were seeded in a 96-well plate, into which various concentrations (0–50 μM) of probe L were added. After 24 h, 10 μL of MTT (5 mg/mL) was added to each well and then incubated for an additional 4 h. Subsequently, DMEM medium was removed, and 100 μL of DMSO was added. Finally, absorbance at 490 nm of the cells was measured using a microplate reader.

2.5. Fluorescence cell imaging

Prior to imaging of exogenous Hg^{2+} and GSH, HeLa cells (1×10^5 cells/mL) were seeded in a plate for 24 h. After that, the medium was removed, and the cells were washed with PBS, incubated with 50 μM L at 37 °C for 30 min, and then washed again with PBS. The cells were subsequently incubated with 5 μM $Hg(ClO_4)_2$ at 37 °C for various time periods (1, 2, 5, 10, 15, 20, or 30 min) and were then subjected to fluorescence imaging at λ_{ex} = 488 nm and λ_{em} = 500–550 nm (green). Similar procedures were used in the imaging of exogenous GSH.

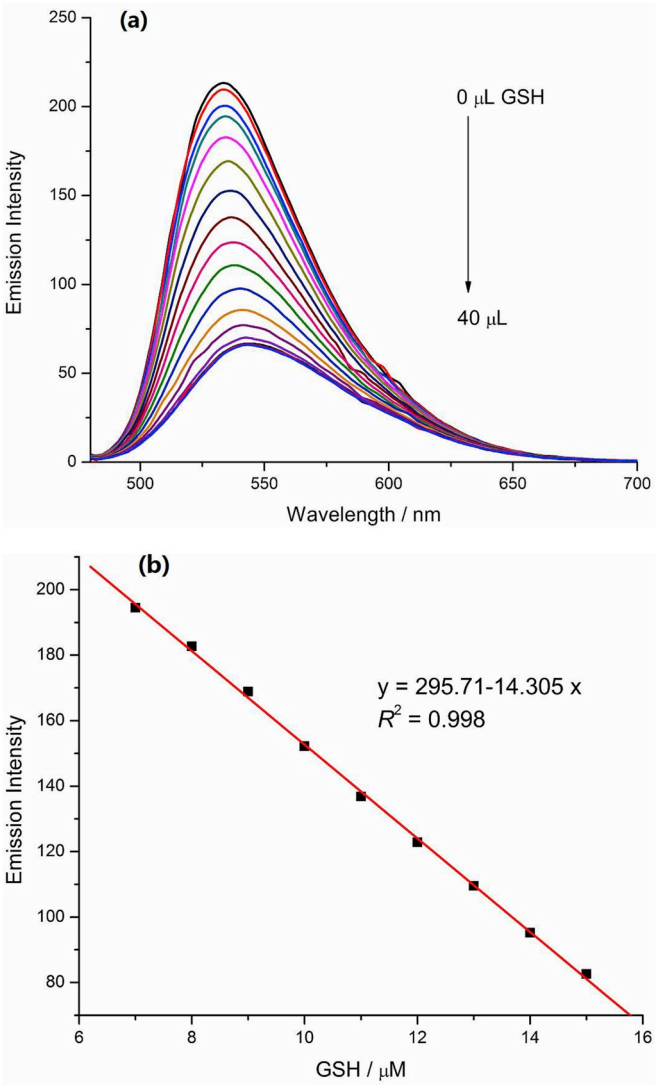

Fig. 4. Fluorescence emission spectra of 20 μM L-Hg^{2+} in the presence of GSH (1 mM, 0–40 μL). The measurement was carried out in 10 mM HEPES buffer, pH 7.4 containing 5% CH_3CN. (b) A linear relationship between fluorescence intensity at 530 nm and GSH concentration.

Co-localization fluorescence imaging was also conducted. HeLa cells were co-stained with Hoechst 33258 (10 μM; a nucleus stain), BODIPY TR ceramide (10 μM; a Golgi complex stain), LysoTracker Red DND-99 (10 μM; a lysosome tracker), Mito-Tracker Red (10 μM; a mitochondrial tracker), and compound L (100 μM) at 37 °C. Prior to imaging, the cells were washed three times with PBS. The confocal fluorescence imaging of stained cells was carried out at λ_{ex} = 488 nm and λ_{em} = 500–550 nm (green) and at λ_{ex} = 639 nm and λ_{em} = 680–780 nm (red).

3. Results and discussion

3.1. Detection of Hg^{2+}

Selectivity is a critical factor for evaluating the performance of a new fluorescent probe. For its application in environmental and biomedical fields, it is crucial that a probe is highly selective to its target rather than to other competing species. The selectivity of compound L towards common metal ions was monitored through fluorescence spectral characteristics (λ_{ex} = 470 nm). The measurements were carried out in a 10 mM HEPES buffer, pH 7.4 containing 5% CH_3CN.

As shown in Fig. 1, free probe L exhibited low emission intensity at 530 nm. When 1 mol equivalence of Hg^{2+} was mixed with the probe, the fluorescence intensity was sharply increased by about 50 folds after 3 min. By contrast, a negligible increase of fluorescence intensity was observed when Na^+, K^+, Ca^{2+}, Mg^{2+}, Zn^{2+}, Cu^{2+}, Fe^{3+}, Fe^{2+}, Co^{2+}, Ni^{2+}, Cd^{2+}, Pb^{2+} or Cr^{3+} at 1 mol equivalence was added. Competitive experiments were also carried out by addition of 1 mol equivalence of Hg^{2+} to a solution containing probe L, Ca^{2+}, Na^+ and Mg^{2+}. The results showed that the selectivity of L towards Hg^{2+} remained unaffected, although a number of other metal ions were presented.

Furthermore, Hg^{2+} titration experiment was carried out. Fig. 2a shows the fluorescence spectra (λ_{ex} = 470 nm) of L incubated with different concentrations of Hg^{2+}. The fluorescence intensity at 530 nm increased in a [Hg^{2+}]-dependent manner; it increased with increasing concentration of Hg^{2+}, reaching its maximum value when 0.5 mol equivalence of Hg^{2+} was added (Fig. 2b). Additionally, the fluorescence intensity increases linearly with the Hg^{2+} concentration range of 0–10 μM. Fluorescence intensity was enhanced by a factor of ~50 when the mole ratio ([Hg^{2+}]/[L]) was 0.5:1, and higher $[Hg^{2+}]_{total}$ did not result in further fluorescent changes. The fluorescence titration experiments further showed that the minimum concentration of Hg^{2+} that could be detected was 27 nM [40] (Fig. S3, Supporting Information).

Moreover, a Job's plot was adopted to determine the binding stoichiometry of L-Hg^{2+} complex. The plot shown in Fig. S4, Supporting Information indicates that when the molar fraction of [Hg^{2+}]/([L] + [Hg^{2+}]) reached 0.5, a maximum fluorescence emission intensity was observed, indicating that the binding between probe L and Hg^{2+} 1:1. Furthermore, the electrospray mass spectrometry and isotope modeling were employed (Figs. S4a and S4b, Supporting Information). The fragment peak of ES-MS at *m/z* 847.25, which corresponds to [(L-H) + Hg^{2+} + $2H_2O$]$^+$ (calculated as 847.25), further confirmed that L formed a 1:1 complex with Hg^{2+}. Using the linear Benesi-Hildebrand equation, a linear relationship between [I_0/(I-I_0)] (at 530 nm) and 1/[Hg^{2+}], which is the fluorescence titration profile, was obtained (Fig. S5, Supporting Information). The association constant for L-Hg^{2+} determined from the slope and the intercept of the plot was $K_{ass} = 4 \times 10^6\ M^{-1}$ [31].

3.2. Selective fluorescence response of L-Hg^{2+} toward GSH/Cys

The selectivity of L towards Hg^{2+} was examined in the presence of a variety of other metal species and amino acids that were widely distributed in biological system, including F^-, Cl^-, Br^-, CH_3COO^-, CO_3^{2-}, NO_3^-, PO_4^{3-}, SO_4^{2-}, PPi, glycine, histidine, aspartic acid, tyrosine, threonine, GSH, Cys, and GSSG. As illustrated in Fig. 3, there were no apparent fluorescence changes upon the addition of species other than GSH and Cys. The fluorescence intensity drastically decreased (by more than 80%) when 1 equiv. of GSH or Cys was added to the solution of L-Hg^{2+}, which suggests that biothiols like GSH and Cys can effectively quench the fluorescence of L-Hg^{2+}. Additionally, in the presence of GSH, the change of fluorescence of Hg^{2+} was visible under natural light or ultraviolet light (365 nm) (Fig. S6, Supporting Information).

We further examined the fluorescence intensity change of L-Hg^{2+} under different GSH concentrations and the result is shown in Fig. 4. The fluorescence intensity of L-Hg^{2+} gradually decreased with the increase of GSH concentration from 0 to 20 μM. In addition, the fluorescence was almost completely quenched when GSH concentration was 18 μM (Fig. 4a). A good linear relationship with a correlation coefficient of 0.998 was observed between the fluorescence quenching and the concentration of GSH (7–15 μM). The relationship can be used for the quantification of GSH (Fig. 4b). The LOD of L-Hg^{2+} in GSH detection determined at 3σ was as low as 0.3 μM, which is lower than commercial glutathione assay kit with its minimum detection content of 1 μM.

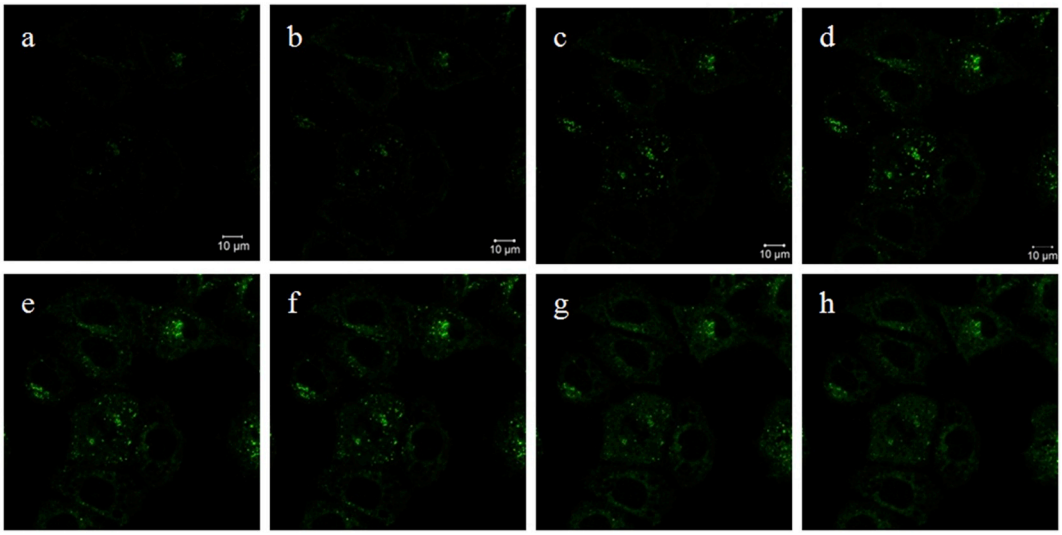

Fig. 5. Confocal fluorescence images of living HeLa cells. HeLa cells was incubated with L (50 μM) at 37 °C for 30 min, followed by $Hg(ClO_4)_2$ (5 μM) for 30 min. (a–h): fluorescence images at 0, 1, 2, 5, 10, 15, 20, and 30 min, respectively. The images were acquired in the green channel (λ_{em} = 500–550 nm). λ_{ex} = 488 nm scale bars = 10 μm. (For interpretation of the references to colour in this figure legend, the reader is referred to the Web version of this article.)

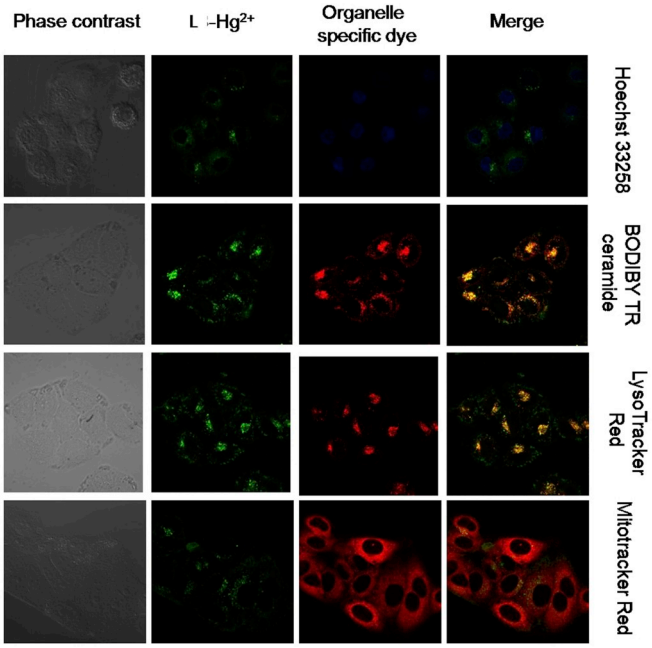

Fig. 6. Confocal microscopic images of HeLa cells, demonstrating colocalization of L-Hg^{2+} and other organelle-specific dyes. Left column: bright-field images. Top to bottom: HeLa cells incubated with Hoechst 33258, BODIPY TR ceramide, LysoTracker Red, and Mitotracker Red, respectively for 30 min at 37 °C, followed by L (50 μM) for 30 min and Hg^{2+} (5 μM) for 15 min. Scale bars = 10 μm. (For interpretation of the references to colour in this figure legend, the reader is referred to the Web version of this article.)

3.3. Fluorescence imaging in living cells

To evaluate potential application of probe L in biological system, its cytotoxicity in the concentration range of 6.25–50 μM was examined by MTT assay (Fig. S7, Supporting Information). The result showed that viability of HeLa cell was higher than 85% after being incubated with different concentrations of probe L for 24 h. The result indicates that probe L has negligible cytotoxicity and high cytocompatibility, thus is suitable for cell imaging.

Consequently, we explored the ability of L in fluorescence imaging of Hg^{2+} in living cells. HeLa cells were first incubated with L (50 st all cells were stained, and stronger fluorescence intensity was observed (Fig. 5). The fluorescence reached its maximum intensity on after about 15 min. The fluorescence reached its maximum intensity on after about 15 min. Mean fluorescence intensity at different incubation times can be found in Fig. S8, Supporting Information. This result indicates that L can penetrate through the cell membrane and distribute in the cytoplasm. Additionally, Hg^{2+} can bind to L, thereby causing the increase of fluorescence intensity inside the cells. However, in an *in vitro* experiment, significant change of fluorescence intensity was not observed when $Hg(ClO_4)_2$ was added into L pre-treated with 10 eq. GSH. This observation may be due to that Hg^{2+} has a stronger binding affinity for GSH than L. It also suggests that the sites that L occupied in cells do not overlap the location of endogenous GSH in HeLa cells. Furthermore, we inactivated endogenous GSH using NEM, a sulfhydryl blocker [41] and then incubated with $Hg(ClO_4)_2$ for a certain period of time. The result showed that the fluorescence change of the complex was negligible compared with that of the control group. These findings suggest that L is a promising sensitive Hg^{2+} probe for cell imaging; the effect of endogenous GSH on the probe is negligible.

In order to further explore other application of L-Hg^{2+} in imaging of living cells, colocalization experiments were conducted in HeLa cells to investigate the organelle-targeting ability of the probe. In this experiment, HeLa cells were co-stained with L-Hg^{2+} and four commercially available probes targeting nucleus (Hoechst 33258), the Golgi apparatus (BODIPY TR ceramide), lysosomes (LysoTracker Red) and mitochondria (Mitotracker Red). As shown in Fig. 6, compared to that of nucleus and mitochondrial, red fluorescence signal of BODIPY TR ceramide in the Golgi apparatus (second row) and that of LysoTracker Red in lysosome (third row) are better overlapped with the green fluorescence of L-Hg^{2+}. Image J was used to calculate the colocalization coefficient, and the Pearson's method was employed to evaluate the colocalization [42]. The colocalization coefficients for L-Hg^{2+} and BODIPY TR ceramide and LysoTracker Red were 0.7 and 0.67, respectively, indicating that the L-Hg^{2+} has high specificity for the Golgi apparatus.

3.4. Practical application of L-Hg^{2+} in human serum and FBS

To evaluate the sensing capability of L-Hg^{2+} in real samples, the probe was applied to detect GSH in FBS and human serum. Based on the correlation between fluorescence intensity and GSH concentration, we

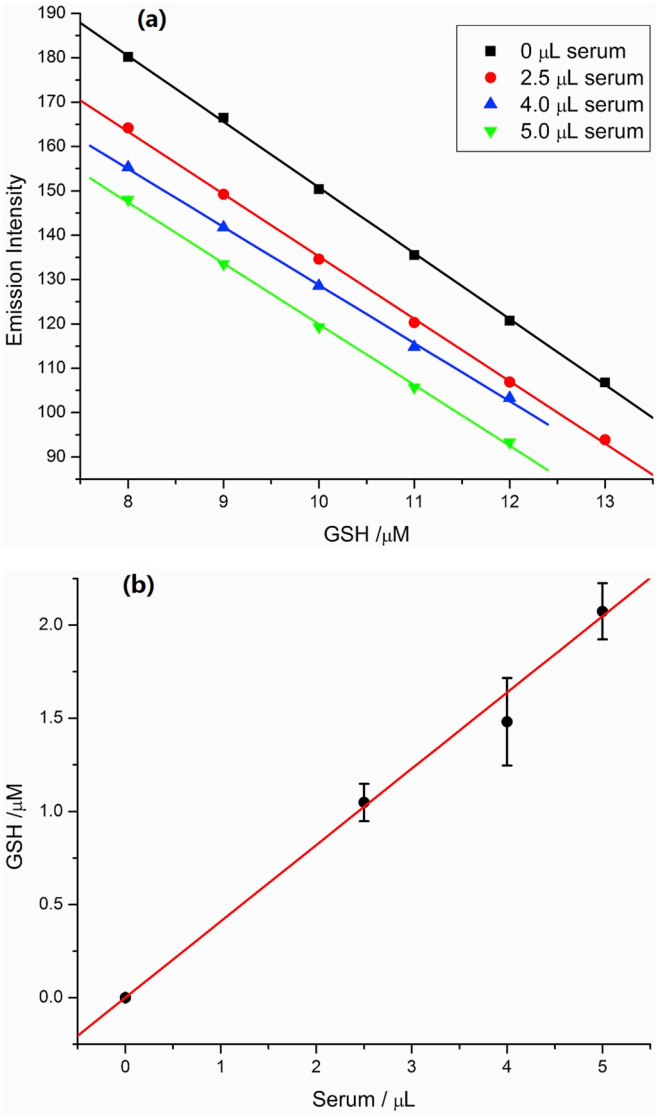

Fig. 7. (a) Fluorescence intensities (λ_{em} = 530 nm) of L-Hg^{2+} in the presence of different concentrations of GSH and varying volumes of human serum. (b) The correlation between calculated GSH concentration and volume of human serum.

adopted the standard addition method, in which specific volume of serum was pre-added before conducting the fluorescence titration of GSH (1 mM), to determine GSH level in human serum by using L-Hg^{2+} (Fig. 7) [43]. Three different volumes of serum (2.5, 4.0, and 5.0 μL) were used. The results were represented as a plot of concentration of added standard (x axis) and fluorescence intensity (y axis) (Fig. 7a). After applying the dilution factors to the samples, we found that the concentration of GSH in human serum was 810 μM (Fig. 7b). The value is within the range of the previously reported value of GSH in healthy subjects (400–1200 μM) [44–46]. The concentration of GSH in FBS was also determined using the same procedure; it was found to be approximately 617 μM (Fig. S9, Supporting Information).

4. Conclusion

In summary, we successfully synthesized an NBD-based "turn-on" fluorescent probe L for Hg^{2+} detection. The probe could rapidly respond to Hg^{2+} in aqueous solution and had high sensitivity with an LOD = 27 nM. It could be applied to monitor exogenous Hg^{2+} in living HeLa cells, which contain abundant GSH whereas no interference. The colocalization experiments further demonstrated that the probe L was able to detect Hg^{2+} in the Golgi apparatus, making it a promising tool for study the function of Golgi involved the metabolism and detoxication of mercury. Lastly, the complex L-Hg^{2+} had high selectivity towards biothiols such as GSH, with the LOD of 0.3 μM, which is much lower than the commercial glutathione assay kit analysis method, usually 1 μM. On this basis, the probe L was easily and successfully employed to detect GSH in FBS and human serum, therefore can be a useful tool for monitoring GSH in a biological system.

Conflicts of interest

The authors declare that they have no conflict of interest.

Acknowledgements

This work is supported by the National Natural Science Foundation of China (21527809, 21775069 and 21976080).

Appendix A. Supplementary data

Supplementary data to this article can be found online at https://doi.org/10.1016/j.talanta.2019.120311.

References

[1] S.M. Ullrich, T.W. Tanton, S.A. Abdrashitova, Mercury in the aquatic environment: a review of factors affecting methylation, Crit. Rev. Environ. Sci. Technol. 31 (2001) 241–293.
[2] O. Regnell, C.J. Watras, Microbial mercury methylation in aquatic environments: a critical review of published field and laboratory studies, Environ. Sci. Technol. 53 (2019) 4–19.
[3] Y. Li, J. Zhao, H. Zhong, Y. Wang, H. Li, Y.-F. Li, V.L. Nguyen, T. Jiang, Z. Zhang, Y. Gao, Z. Chai, Understanding enhanced microbial MeHg production in mining-contaminated paddy soils under sulfate amendment: changes in Hg mobility or microbial methylators? Environ. Sci. Technol. 53 (2019) 1844–1852.
[4] W. Cui, G. Liu, M. Bezerra, D.A. Lagos, Y. Li, Y. Cai, Occurrence of methylmercury in rice-based infant cereals and estimation of daily dietary intake of methylmercury for infants, J. Agric. Food Chem. 65 (2017) 9569–9578.
[5] J.N.M. Commandeur, N.P.E. Vermeulen, Molecular and biochemical mechanisms of chemically induced nephrotoxicity: a review, Chem. Res. Toxicol. 3 (1990) 171–194.
[6] A.L.V. Milioni, B.V. Nagy, A.L.A. Moura, E.C. Zachi, M.T.S. Barboni, D.F. Ventura, Neurotoxic impact of mercury on the central nervous system evaluated by neuropsychological tests and on the autonomic nervous system evaluated by dynamic pupillometry, NeuroToxicology 59 (2017) 263–269.
[7] Y.-X. Gao, H. Zhang, X. Yu, J. He, X. Shang, X. Li, Y. Zhao, Y. Wu, Neurodevelopmental effect resulting from consumption of marine fish from a coastal archipelago in China, J. Agric. Food Chem. 62 (2014) 5207–5213.
[8] G. Qiu, X. Feng, S. Wang, L. Shang, Mercury and methylmercury in riparian soil, sediments, mine-waste calcines, and moss from abandoned Hg mines in east Guizhou province, southwestern China, Appl. Geochem. 20 (2005) 627–638.
[9] X. Wang, Z. Ye, B. Li, L. Huang, M. Meng, J. Shi, G. Jiang, Growing rice aerobically markedly decreases mercury accumulation by reducing both Hg bioavailability and the production of MeHg, Environ. Sci. Technol. 48 (2014) 1878–1885.
[10] B. Li, J. Shi, X. Wang, M. Meng, L. Huang, X. Qi, B. He, Z. Ye, Variations and constancy of mercury and methylmercury accumulation in rice grown and contaminated paddy field sites in three provinces of China, Environ. Pollut. 181 (2013) 91–97.
[11] J. Chen, Y. Wang, X. Wei, P. Xu, W. Xu, R. Ni, J. Meng, Magnetic solid-phase extraction for the removal of mercury from water with ternary hydrosulphonyl-based deep eutectic solvent modified magnetic graphene oxide, Talanta 188 (2018) 454–462.
[12] B. Han, J. Yuan, E. Wang, Sensitive and selective sensor for biothiols in the cell based on the recovered fluorescene of the CdTe quantum dots-Hg(II) system, Anal. Chem. 81 (2009) 5569–5573.
[13] X. Zhu, Z. Zhao, X. Chi, J. Gao, Facile, sensitive, and ratiometric detection of mercuric ions using GSH-capped semiconductor quantum dots, Analyst 138 (2013) 3230–3237.
[14] F. Yu, P. Li, B. Wang, K. Han, Reversible near-infrared fluorescent probe introducing tellurium to mimetic glutathione peroxidase for monitoring the redox cycles between peroxynitrite and glutathione in vivo, J. Am. Chem. Soc. 135 (2013) 7674–7680.
[15] F. Yu, P. Li, P. Song, B. Wang, J. Zhao, K. Han, Facilitative functionalization of cyanine dye by an on-off-on fluorescent switch for imaging of H_2O_2 oxidative stress and thiols reducing repair in cells and tissues, Chem. Commun. 48 (2012) 4980–4982.
[16] B.K. McMahon, T. Gunnlaugsson, Selective detection of the reduced form of

glutathione (GSH) over the oxidized (GSSG) form using a combination of glutathione reductase and a Tb(III)-Cyclen maleimide based lanthanide luminescent 'switch on' assay, J. Am. Chem. Soc. 134 (2012) 10725–10728.
[17] H. Refsum, P.M. Ueland, O. Nygard, S.E. Vollset, Homocysteine and cardiovascular disease, Aun. Rev. Med. 49 (1998) 31–62.
[18] F. Wang, C. Feng, L. Lu, Z. Xu, W. Zhang, A ratiometric fluorescent probe for rapid and sensitive detection of biothiols in fetal bovine serum, Talanta 169 (2017) 149–155.
[19] S.J.S. Flora, N. Dwivedi, U. Deb, P. Kushwaha, V. Lomash, Effects of co-exposure to arsenic and dichlorvos on glutathione metabolism, neurological, hepatic variables and tissue histopathology in rats, Toxicol. Res. 3 (2014) 23–31.
[20] L.H. Lash, Mitochondrial glutathione in toxicology and disease of the kidneys, Toxicol. Res. 1 (2012) 39–46.
[21] J. Du, J. Fan, X. Peng, P. Sun, J. Wang, H. Li, S. Sun, A new fluorescent chemodosimeter for Hg^{2+}: selectivity, sensitivity, and resistance to Cys and GSH, Org. Lett. 12 (2010) 476–479.
[22] C. Zhang, H. Zhang, M. Li, Y. Zhou, G. Zhang, L. Shi, Q. Yao, S. Shuang, C. Dong, A turn-on reactive fluorescent probe for Hg^{2+} in 100% aqueous solution, Talanta 197 (2019) 218–224.
[23] Y. Wang, M. Gao, Q. Chen, F. Yu, G. Jiang, L. Chen, Associated detection of superoxide anion and mercury(II) under chronic mercury exposure in cells and mice models via a three-channel fluorescent probe, Anal. Chem. 90 (2018) 9769–9778.
[24] B. Liu, X. Hu, J. Chai, B. Yang, Aggregation and deaggregation of rhodamine fluorescent probe for sequential recognition of Hg(II) and Cys with green emission, Sens. Actuators B Chem. 228 (2016) 94–100.
[25] M. Nagy, S.L. Kovacs, T. Nagy, D. Racz, M. Zsuga, S. Keki, Isocyanonaphthalenes as extremely low molecular weight, selective, ratiometric fluorescent probes for Mercury(II), Talanta 201 (2019) 165–173.
[26] T. Jiang, B. Ke, H. Chen, W. Wang, L. Du, K. Yang, M. Li, Bioluminescent probe for detecting mercury(II) in living mice, Anal. Chem. 88 (2016) 7462–7465.
[27] Y. Huang, C. Li, W. Shi, H. Tan, Z. He, L. Zheng, F. Liu, J. Yan, A near-infrared BODIPY-based fluorescent probe for ratiometric and discriminative detection of Hg^{2+} and Cu^{2+} ions in living cells, Talanta 198 (2019) 390–397.
[28] K. Bera, A.K. Das, M. Nag, S. Basak, Development of a rhodamine-rhodanine-based fluorescent mercury sensor and its use to monitor real-time uptake and distribution of inorganic mercury in live zebrafish larvae, Anal. Chem. 86 (2014) 2740–2746.
[29] S.R. Bhatta, B. Mondal, G. Vijaykumar, A. Thakur, ICT-isomerization-induced turn-on fluorescence probe with a large emission shift for mercury ion: application in combinational molecular logic, Inorg. Chem. 56 (2017) 11577–11590.
[30] H. Lee, H.S. Lee, J.H. Reibenspies, R.D. Hancock, Mechanism of "turn-on" fluorescent sensors for mercury(II) in solution and its implications for ligand design, Inorg. Chem. 51 (2012) 10904–10915.
[31] L. Chen, L. Yang, H. Li, Y. Gao, D. Deng, Y. Wu, L. Ma, Tridentate lysine-based fluorescent sensor for Hg(II) in aqueous solution, Inorg. Chem. 50 (2011) 10028–10032.
[32] J. Wang, X. Qian, Two regioisomeric and exclusively selective Hg(II) sensor molecules composed of a naphthalimide fluorophore and an o-phenylenediamine derived triamide receptor, Chem. Commun. (2006) 109–111.
[33] L.N. Neupane, J.Y. Park, J.H. Park, K.H. Lee, Turn-on fluorescent chemosensor based on an amino acid for Pb(II) and Hg(II) ions in aqueous solutions and role of tryptophan for sensing, Org. Lett. 15 (2013) 254–257.
[34] X. Wang, Z. Zhang, X. Ma, J. Wen, Z. Geng, Z. Wang, Real-time fluorescence assays of alkaline phosphatase and ATP sulfurylase activities based on a novel PPi fluorescent probe, Talanta 137 (2015) 156–160.
[35] J. Wen, Z. Geng, Y. Yin, Z. Wang, A versatile water soluble fluorescent probe for ratiometric sensing of Hg^{2+} and bovine serum albumin, Dalton Trans. 40 (2011) 9737–9745.
[36] B. Ma, F. Zeng, X. Li, S. Wu, A facile approach for sensitive, reversible and ratiometric detection of biothiols based on thymine-mediated excimer-monomer transformation, Chem. Commun. 48 (2012) 6007–6009.
[37] J.L. Sessler, J.W. Sibert, V. Lynch, Model studies related to hemerythrin. Synthesis and characterization of a bridged tetranuclear iron(III) complex, Inorg. Chem. 29 (1990) 4143–4146.
[38] K. Wieghardt, I. Tolksdorf, W. Herrmann, Coordination chemistry of the bimacrocyclic, potentially binucleating ligand 1,2-bis(1,4,7-triaza-1-cyclononyl) ethane (dtne). Electrochemistry of its first transition series metal(II,III) complexes. Characterization of the new hemerythrin model complex $[Fe_2(dtne)(\mu\text{-}O)(\mu\text{-}CH_3CO_2)_2]Br_2{\cdot}H_2O$, Inorg. Chem. 24 (1985) 1230–1235.
[39] A. Mcauley, P.R. Norman, O. Olubuyide, Preparation, characterization, and outer-sphere electron-transfer reactions of nickel complexes of 1,4,7-triazacyclononane, Inorg. Chem. 23 (1984) 1938–1943.
[40] J. Wen, Z. Geng, Y. Yin, Z. Zhang, Z. Wang, A Zn^{2+}-specific turn-on fluorescent probe for ratiometric sensing of pyrophosphate in both water and blood serum, Dalton Trans. 40 (2011) 1984–1989.
[41] M. Taki, K. Akaoka, S. Iyoshi, Y. Yamamoto, Rosamine-based fluorescent sensor with femtomolar affinity for the reversible detection of a mercury ion, Inorg. Chem. 51 (2012) 13075–13077.
[42] J. Gong, Y. Li, C. Zhang, J. Huang, Q. Sun, A thiazolo[4,5-b]pyridine-based fluorescent probe for detection of zinc ions and application for in vitro and in vivo bioimaging, Talanta 185 (2018) 396–404.
[43] G.G. Ibabe, L. Saa, V. Pavlov, Enzymatic product-mediated stabilization of CdS quantum dots produced in situ: application for detection of deduced glutathione, NADPH, and glutathione reductase activity, Anal. Chem. 85 (2013) 5542–5546.
[44] J.P. Richie, P. Abraham, Y. Leutzinger, Long-term stability of blood glutathione and cysteine in humans, Clin. Chem. 42 (1996) 1100–1105.
[45] J.P. Richie, L. Skowronski, P. Abraham, Y. Leutzinger, Blood glutathione concentrations in a large-scale human study, Clin. Chem. 42 (1996) 64–70.
[46] R. Kand'ar, P. Zakova, H. Lotkova, O. Kucera, Z. Cervinkova, Determination of reduced and oxidized glutathione in biological samples using liquid chromatography with fluorimetric detection, J. Pharm. Biomed. Anal. 43 (2007) 1382–1387.